Chemical Science

ROYAL SOCIETY OF CHEMISTRY

EDGE ARTICLE

View Article Online
View Journal

Cite this: DOI: 10.1039/d5sc06370a

All publication charges for this article have been paid for by the Royal Society of Chemistry

Covalently grafted MOP-on-MOF hybrid ionic-porous composite for efficient adsorption and catalysis

Dipayan Ghosh, [a] Sahel Fajal, [a] Kishalay Biswas, [a] Anirban Roy, [a] Dipanjan Majumder [a] and Sujit K. Ghosh *[ab]

Received 20th August 2025
Accepted 10th November 2025

DOI: 10.1039/d5sc06370a

rsc.li/chemical-science

Development of multifunctional hybrid porous composite materials with significantly enhanced properties is highly desirable; however, it remains challenging due to the lack of proper synthetic strategies. Here, we present a facile design principle to construct multifunctional hybrid ionic porous composite materials through covalent linking of amino pendant nanosized cationic metal–organic polyhedra (MOPs) with an amino-functionalized anionic metal–organic framework (MOF) using dynamic covalent chemistry of strong secondary amide bonds. The optimized MOP-on-MOF hybrid nanocomposite was synthesized *via* covalent grafting, followed by electrostatic-driven assembly of Zr-MOP-NH_2 on the surface of Ti-MIL-125-NH_2 using a series of organic linkers. The developed nanocomposites revealed tunable enhanced physicochemical properties with intact crystal structure, morphology, porosity, and stability of the parent MOF, while effectively preventing the aggregation and leaching of MOPs. Importantly, the hybrid nanocomposite demonstrated significantly improved selective adsorption properties toward polyiodide species in water, which is important from the point of view of radioiodine sequestration from water, and served as a potential platform for efficient heterogeneous catalysis toward Lewis acid-mediated phosphate-ester hydrolysis of toxic nerve agents with high product selectivity and good recyclability. This unique covalently grafted MOP-on-MOF strategy offers a promising means of introducing novel multifunctional robust porous composite materials for various potential applications.

Introduction

Enhanced selective adsorption and catalytic conversion of target molecules with high efficiency have always been of considerable research interest in both academia and industry. In this regard, by virtue of reticular chemistry, in the last few decades, the development of various advanced functional porous materials for efficient adsorbents and catalysts has skyrocketed.[1–5] Among these, crystalline extended porous structures such as metal–organic frameworks (MOFs) and covalent organic frameworks (COFs) are being widely investigated, due to their outstanding structural diversity, tunable functionality, and versatility, which make them potential candidates for guest adsorption and heterogeneous catalysis.[1–9] Apart from these, metal–organic polyhedra (MOPs), inorganic–organic hybrid discrete porous coordination cages made up of metal ions (or clusters) and polydentate directional organic linkers, are another class of advanced functional porous materials that have also been the subject of significant research interest during the past decade.[10–12,18,19] The molecular characteristics of MOPs and their customized hybrid metal–organic surfaces, featuring distinct structures and unique symmetries, provide these materials with diverse orthogonal reactivity. Additionally, the quantity and placement of particular functional groups on the surface of MOPs can be accurately determined. This allows for precise control over their processability and chemical reactivity while preserving their porous nature.[12,13] Such a unique combination of intrinsic porosity with distinct surface reactivity is what makes MOPs a central focus in various applications, such as separation, catalysis, storage, sensing, biology, *etc.*[10–16,19] Nevertheless, despite possessing certain distinct benefits like solubility and processability, the usage range of the majority of MOPs is constrained by their robust intermolecular interactions and low surface area. Moreover, the majority of MOPs are observed to possess poor chemical stability, restricting their real-world applicability in aqueous or chemical environments.[17–19] In this regard, for instance, Zr(IV)-based MOPs have recently gained recognition for their enhanced chemical stability, thus demonstrating significant potential for adsorption and catalysis.[20–24] However, due to the inevitable aggregation-induced obstruction of the active sites, when the guest is taken out in the solid phase, regrettably,

[a]Department of Chemistry, Indian Institute of Science Education and Research (IISER) Pune, Dr Homi Bhaba Road, Pashan, Pune 411008, India. E-mail: sghosh@iiserpune.ac.in

[b]Centre for Water Research (CWR), Indian Institute of Science Education and Research (IISER) Pune, India

MOPs are still far from their potential effectiveness.[17–19] Therefore, finding a robust solution to construct MOP-based materials addressing the aforementioned issues is a highly desirable research topic. In this context, development of MOP-based hybrid composite porous materials with high porosity and stability by a facile synthetic strategy, without compromising the inherent properties, serves as an optimal solution.

In recent years, regulated molecular engineering has enabled the growth of advanced functionalities of numerous composite porous materials, which are created by combining the best qualities and maximizing the performance of various advanced porous materials.[25,26] Among these, porous hybrid nanocomposites have gained a lot of attention and taken center stage since they have allowed for the development of distinctive and multipurpose platforms that enable the realization of desired applications.[27–29] Out of them, recently, advanced porous hybrid nanocomposites composed of MOFs and MOPs have caught significant attention with excellent performance in catalysis, adsorption, and other areas.[29–39] MOFs are inorganic–organic hybrid crystalline extended porous coordination polymers constructed with metal ions/nodes and organic ligands and garnered significant recognition due to their structural and compositional diversity and remarkable tunability in pore characteristics.[40–42] To date, the reported strategies for

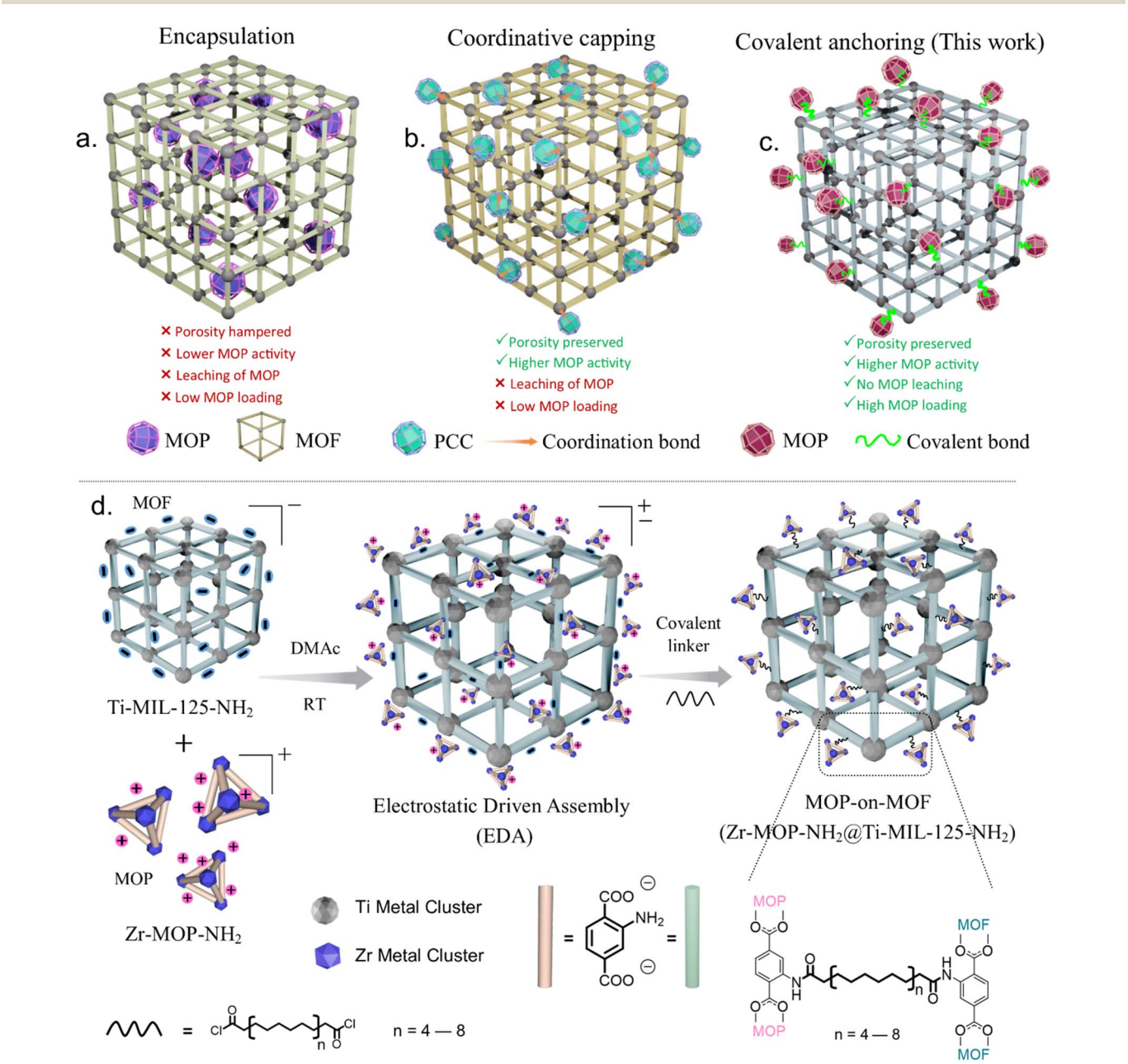

Fig. 1 Schematic illustration of different strategies used for synthesis of MOP/MOF based composite materials: (a) encapsulation, (b) coordinative capping, and (c) covalent anchoring. (d) Illustration of synthesis of MOP-on-MOF hybrid composites through covalent anchoring, followed by electrostatic driven assembly.

fabrication of MOF and MOP based nanocomposites can be briefly summarized as (1) encapsulation of MOPs inside the porous cavity of MOFs and (2) coordination capping of MOPs (or porous coordination cages, PCCs) on the surface of MOFs (Fig. 1a and b).[32,38,39] Among them, although the encapsulation strategy explored the tunable physicochemical properties of the host MOFs and significantly addressed the aggregation and solubility issues of the MOPs, the porosity of the hybrid was found to be compromised. This is mainly due to the random arrangement of MOPs within the host (MOFs) cavity. Furthermore, the stability of the hybrid composite under harsh circumstances may be a concern due to the non-covalent interactions between the guest MOP and host MOF.[38] On the other hand, the coordination anchoring "cage-on-MOF" strategy is suitable for a large number of MOPs (or PCCs), homogeneous capping with the external surface of MOFs to produce highly porous hybrid materials. It is noteworthy that this approach has also handled MOPs' self-aggregation and solubility concerns and further explored the maximum potential of MOPs owing to their outer surface decoration. However, the relatively weak coordination interaction between the functional group of MOPs and surface-exposed metal sites of MOFs, leaching of MOPs from the composite materials under acidic/basic, polar, and mixed organic solvent conditions, may be a concern for their real-time large-scale application. Moreover, the strategy indicated a relatively low MOP loading capacity on the surface of MOFs.[38,39]

Herein, for the first time, we report a novel covalent grafting strategy, followed by electrostatic-driven assembly (EDA) to construct MOP-on-MOF based hybrid porous composites through strong covalent bond formation between the functional ligands of MOPs and MOFs (Fig. 1c and d). This covalent anchoring strategy explored the homogeneous distribution of nano-sized functional MOPs throughout the surface of MOFs with robust bonding interaction, and the inherent properties of both the MOPs and MOFs were found to be intact within the composite material. The strategy typically includes two steps: first, assembly of positively charged MOPs on the outer surface of an anionic MOF through electrostatic-driven assembly (EDA) and second, linking and positioning of MOPs with the MOF surface through covalent chemistry using small organic linkers (Fig. 1d). As a proof of concept, herein, we choose Zr-MOP-NH_2 as the guest[43] and Ti-MIL-125-NH_2 (ref. 44–47) as the host matrix, respectively. The rationally selected chemically stable Zr-MOP-NH_2 ($\{[Cp_3Zr_3O(OH)_3]_4(NH_2\text{-}BDC)_6\}Cl_4$ Cp = cyclopentadienyl ligand NH_2BDC = 2-aminoterephthalic acid) features a nanosized structure, which is ideal for homogeneous distribution throughout the surface of the MOF, while the cationic nature helps in EDA. Additionally, the free amino (–NH_2) group of the ligand in Zr(IV)-MOP enables covalent linkage with other organic moieties. On the flip side, the host, Ti-MIL-125-NH_2, exhibited a highly porous, stable and negatively charged structure (due to the polar –OH/–O moiety of the $Ti_8O_8(OH)_4$ cluster) with the pendent –NH_2 group on its surface, which is ideal for the target nanocomposite preparation. Optimizing the strategic synthesis to control the electrostatic interaction between the MOP and MOF, we employed a long-chain acid chloride ligand as a bimodal connector to covalently join the MOPs on the outer surface of the MOF through the formation of a strong secondary amide bond (Fig. 1d). Notably, our protocol explored the formation of an effective MOP-on-MOF nanocomposite without compromising the porosity significantly and retained the integrity as well as the properties of the individual materials at their maximum. Most importantly, the leaching issue of MOPs from the surface of the MOF in the composite was fully addressed by this covalent anchoring strategy. The developed cationic MOP-on-MOF nanocomposite (Zr-MOP-NH_2@Ti-MIL-125-NH_2), named IPM-405 (IPM stands for IISER Pune Material), was found to be highly effective towards selective adsorption and heterogeneous catalysis, as exemplified by ultrafast, recyclable, selective sequestration of polyiodide species (*i.e.*, triiodide I_3^-) from water and Lewis acid mediated phosphate-ester hydrolysis of toxic nerve agents, respectively.

Results and discussion

We strategically chose a trinuclear Zr(IV) cluster-based cationic amino pendant Zr-MOP-NH_2 (named Zr-MOP)[43] as the cage of choice due to its aqueous phase stability, tailored functionality, selective adsorption, and catalytic behavior.[37,63] To anchor these nanosized (~2 nm) Zr-MOPs on the porous host, Ti-MIL-125-NH_2 (named Ti-MOF) (a Ti_8 ring-shaped titanium-oxo cluster connected amino functionalized MOF) was rationally selected as the host porous matrix. Ti-MOF has been considered an ideal host matrix owing to its large surface area, well-defined particle morphology, and exceptional framework stability, which stems from its robust Ti(IV)–O bonds.[45] Both Zr-MOP and Ti-MOF were synthesized (Sections S2.1 and S2.2) and characterized as per the reported procedure (Fig. 2a–c and S1–S6).

Thereafter, to covalently anchor these Zr-MOPs on the Ti-MOF surface, a certain amount of activated Ti-MOF and Zr-MOP was taken in a vial. To obtain an adequate interaction between the Zr-MOP and Ti-MOF, both of them were mixed in a solvent for an optimum time. Under these conditions, there was an electrostatic interaction between the Zr-MOP and the Ti-MOF surface. The negative surface charge of the Ti-MOF enhances the adsorption of these cationic nanosized MOPs and electrostatically assembles them on its external surface (Fig. 1d). Then, to form the covalent interaction, a quantitative amount of bidentate flexible acid chloride ligand was added to the reaction system at room temperature under mild stirring conditions. The free amino groups of both systems react with the acid chloride ligand, and this long-chain bidentate acid chloride ligand acts as a connector between these MOPs and the Ti-MOF surface *via* the formation of a strong secondary amide bond (Fig. 1d, see Section S2.3 for details). After completion of the reaction, the expected MOP-on-MOF product was collected and washed properly to remove the unbound MOPs and dried under a vacuum oven.

After the synthesis, the composite named IPM-405 has been characterized in detail. At first, the powder X-ray diffraction (PXRD) analysis of IPM-405 was performed, which demonstrates the high crystalline nature of IPM-405 (Fig. 2a). The

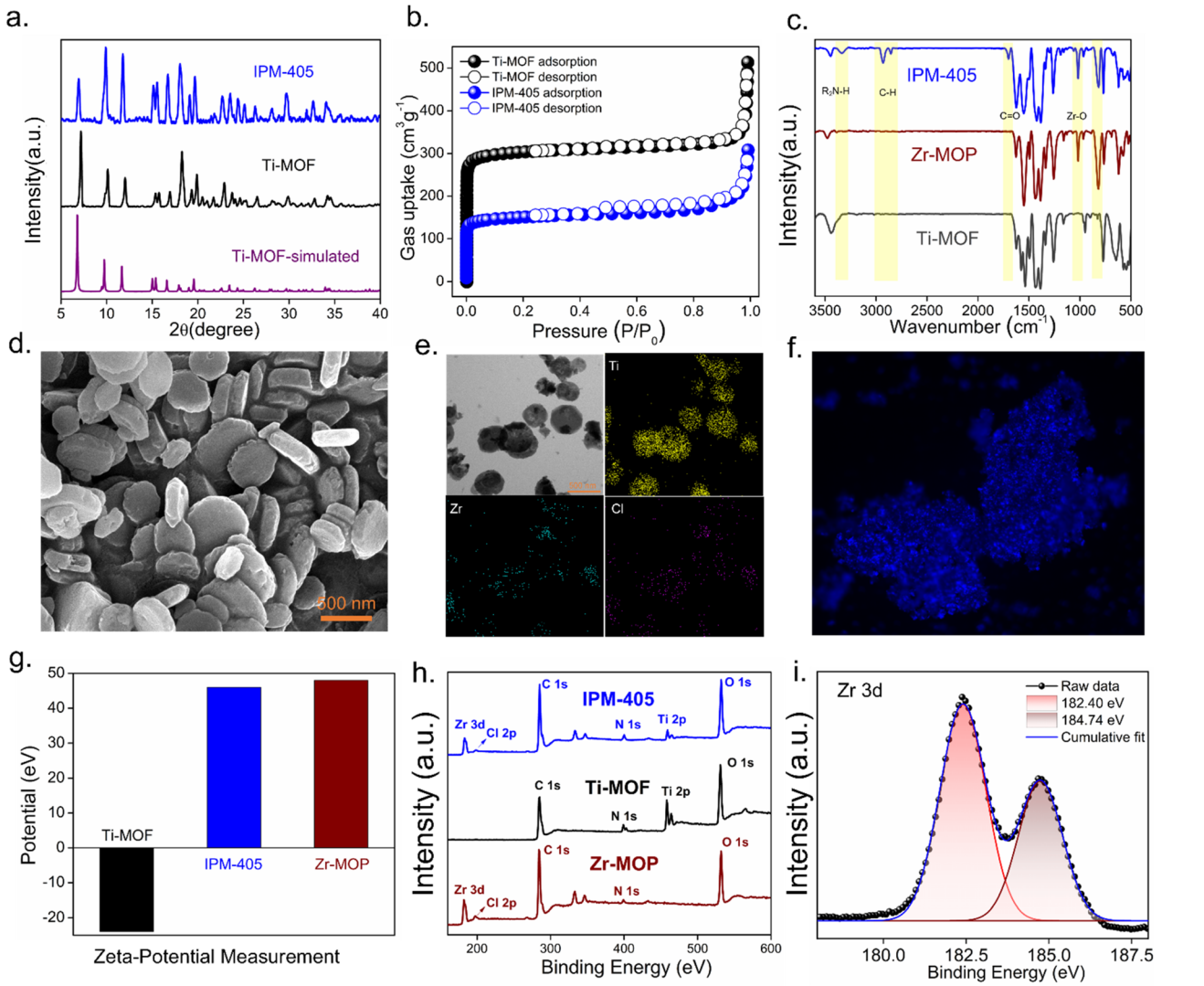

Fig. 2 (a) PXRD, (b) N_2@77 K of IPM-405 and Ti-MOF, and (c) FT-IR spectra of IPM-405 along with pristine Zr-MOP and Ti-MOF. (d) FESEM image of IPM-405. (e) TEM elemental mapping of IPM-405. (f) fluorescence microscopy image of IPM-405 showing its highly emissive nature. (g) Zeta-potential and (h) XPS survey spectra of IPM-405 with the pristine Ti-MOF and Zr-MOP. (i) Zr 3d deconvoluted XPS spectra of IPM-405.

diffraction peak matches with that of Ti-MOF, referring to the retained integrity of the pristine MOF. The low-temperature nitrogen gas adsorption isotherm (77 K) of the material indicates significant gas uptake at low pressure, depicting the porous nature of the composite (Fig. 2b). Consequently, the BET surface area and pore diameter of IPM-405 (surface area 535 m^2 g^{-1}) have been decreased compared to those of Ti-MOF (surface area 1005 m^2 g^{-1}) (Fig. S7). This is because of the presence of the Zr-MOP on the Ti-MOF surface in the composite. Also, the gas adsorption data demonstrate a typical type-I adsorption isotherm, indicating the microporous nature of the material. The Fourier transform infrared spectroscopy (FT-IR) analysis of the hybrid composite was performed (Fig. 2c and S8). The appearance of these corresponding IR stretching bands at 1705 cm^{-1} (C═O of the secondary amide bond), 1544 cm^{-1} (corresponds to an interaction of the ν(C–N) and the δ(CNH) vibrations) and 1305 cm^{-1} (δ(NH) and δ(OCN) of the secondary amide bond) in IPM-405 signifies the formation of secondary amide bond after the reaction of free –NH_2 moieties of the materials with the acid-chloride functionality of the connector.[48] The reduction of the primary amine peak at 3500 cm^{-1} and the presence of a new secondary amide (N–H) single band at 3344 cm^{-1} further support the successful formation of this secondary amide bond in IPM-405. Moreover, the appearance of IR bands at 2700 cm^{-1} corresponds to the C–H stretching of the long alkane chain, reflecting the presence of this long-chain acid chloride linker in the composite. Additionally, the IR band at 1040 cm^{-1} indicates the presence of a Zr–O bond similar to that in pristine Zr-MOP (Fig. 2c and S8). Furthermore, to characterize this secondary amide bond, the digested ^{1}H-NMR of the composite was performed; the Nuclear Magnetic Resonance (NMR) spectra supported the presence of secondary amide functionality (S9 and 10).[48] Thereafter, the morphological characterization of the hybrid composite was performed. The FESEM and TEM analysis of IPM-405 has depicted a similar coin-shaped particle identical to pristine Ti-

MOF (Fig. 2d) and (S11–S15). Interestingly, the outer surface of the particles appeared rougher than that of Ti-MOF. This might be because of the distribution of the Zr-MOP on the surface of Ti-MOF in the hybrid composite. To further investigate, FESEM-EDX mapping was performed. This indicates the homogeneous distribution of relevant elements (Zr and Cl) throughout the composite surface (S17 and 18). Furthermore, to investigate at higher resolution, TEM-EDX analysis was performed. This also shows a similar homogeneous distribution of Zr and Cl throughout the surface of IPM-405 (Fig. 2e, S20 and 21). Interestingly, the line-scan TEM-EDX mapping demonstrates that Zr and Cl were present only on the Ti-MOF surface (S23). This validates the homogeneous anchoring of Zr-MOP on the surface of Ti-MOF. Next, in order to investigate the surface roughness, the Atomic Force Microscopy (AFM) measurement of the sample was performed. This further revealed that IPM-405 exhibits a rougher surface morphology compared to Ti-MOF (S24 and S25). Thereafter, to investigate the surface interaction of the Zr-MOP and the Ti-MOF, zeta-potential measurement was performed. The Zr-MOP carries a positive charge($\{[Cp_3Zr_3O(OH)_3]_4(NH_2\text{-}BDC)_6\}Cl_4$), while the Ti-MOF has a negative charge (due to the polar –OH/–O moiety of the $Ti_8O_8(OH)_4$ cluster). In contrast, IPM-405 exhibits a positive surface charge (Fig. 2g and S26). This observation indicates successful anchoring of cationic Zr-MOPs onto the negative surface of Ti-MOF to construct the hybrid composite. Furthermore, the hybrid composite reflects a strongly emissive nature under fluorescence microscopy, due to the presence of strongly emissive Zr-MOP on the surface of Ti-MOF (Fig. 2f and S28).[37] Other optical characterization studies, such as solid-state ultraviolet-visible diffuse reflectance spectroscopy (DRS) and solid-state photoluminescence spectroscopy (PL), have been performed (Fig. S29 and 30). In solid-state PL, IPM-405 has also reflected a strong emission at 500 nm, indicating its high fluorescence in nature, coming from the presence of strongly emissive Zr-MOPs. Thereafter, to investigate in detail, XPS analysis was performed. The XPS survey spectra have demonstrated the presence of Zr and Cl in the composite, indicating the presence of Zr-MOPs on the surface of the Ti-MOF in the hybrid composite (Fig. 2h, S31 and 32). In the deconvoluted Zr 3d XPS spectra, there was a significant shift towards higher binding energy in IPM-405 compared to the pristine Zr-MOP (Fig. 2i and S31), which signifies the electrostatic interaction between the cationic Zr-MOP and the anionic Ti-MOF surface. Similarly, a significant shift in Ti 3d deconvoluted XPS spectra of IPM-405 was observed compared to pristine Ti-MOF, which further supports this electrostatic interaction (Fig. S33). In the deconvoluted N 1s spectra of IPM-405, the N 1s peak corresponding to this secondary amide nitrogen and primary amine nitrogen has also been found to reflect (Fig. S35). Then, to calculate the amount of Zr anchoring in the composite, the ICP-MS analysis of the digested sample was performed, and it was calculated that around 50 wt% of Zr was loaded onto Ti-MOF in IPM-405 (Fig. S38). To further verify the importance of the covalent grafting strategy, the leaching test of the composite was performed (see Sections S4, S36–38). The result indicated that no Zr-MOPs were leached from the surface of Ti-MOF after covalent grafting. This demonstrated the necessity to introduce a covalent bond into the formation of the MOP-on-MOF hybrid composite system. Inspired by the above results in order to generalize the covalent grafting strategy, we have further developed a series of MOP-on-MOF composites by using other acid-chloride ligands (C_n, n = 6–10) (see Section S5 and Fig. S39–43). We also performed the possible counter test of the composite fabrication in Sections S8 and S9 and (Fig. S67–87).

Iodine sequestration study in the aqueous phase

In nuclear energy/power plants, iodine is one of the toxic radionuclide wastes generated during nuclear-spent fuel reprocessing.[49] The water discharged from nuclear reactor chiller plants contains a significant amount of radioactive iodine. Because of its high mobility and radiological and biological toxicity, iodine has been considered as a toxic nuclear waste and a great threat to the world from the human health and environmental points of view. So, for sustainable future development of nuclear energy, while considering human health and the environment, sequestration of iodine is highly desirable.[35] Porous materials, including MOFs,[51] COFs,[35] and porous organic polymers (POPs),[54,55] have always been suitable choices for the sequestration of gas-phase iodine because of their high surface area, well-ordered pore structure, tunable functional moiety, and high operational stability. Most of the iodine removal studies that have previously been reported are mainly focused on gas phase capture of iodine.[50–55] On the other hand, aqueous phase iodine sequestration always remains a challenge due to the presence of a large excess of counter anions, aqueous phase stability, and low performance of the material in the aqueous phase.[56–59,65] In this context, the development of iodine-selective adsorbents with fast kinetics, high selectivity, and removal of low/ultra-trace amounts of iodine in the presence of a large excess of counter anions in the aqueous phase is highly desirable but challenging.

We have shown here that the IPM-405 composite demonstrates the presence of discrete cationic Zr clusters with exchangeable Cl^- ions, free $–NH_2$ moieties, hydrophobic long alkane chains, and secondary amide groups, along with other functional moieties (Fig. 3a and S44). Interestingly, all these functionalities are experimentally and theoretically proven to selectively interact with iodine (I_3^-).[35,57] Inspired by this, initially we tested the efficiency of iodine adsorption in the aqueous phase. As a result, IPM-405 shows a rapid sequestration rate for the polyiodide species (I_3^-) in the aqueous phase with ultrafast kinetics, where IPM-405 was able to decontaminate around 95% of 100 ppm (v/m = 1) polyiodide species (I_3^-) within just 1 min (Fig. 3b and S45–S49). Then, to check the selective removal efficiency in the aqueous phase, an iodine (I_3^-) capture study was performed in the presence of a large excess of counter ions. The composite was able to completely sequester 100 ppm (v/m = 1) of tri-iodide species within just 5 min in the presence of a 100-fold excess of counter anions (Cl^-, Br^-, NO_3^-, and SO_4^{2-}) (Fig. 3c and S50–52), which depicts the highly iodine-selective nature of IPM-405. For a sustainable adsorbent, the regeneration ability of the adsorbent is a very

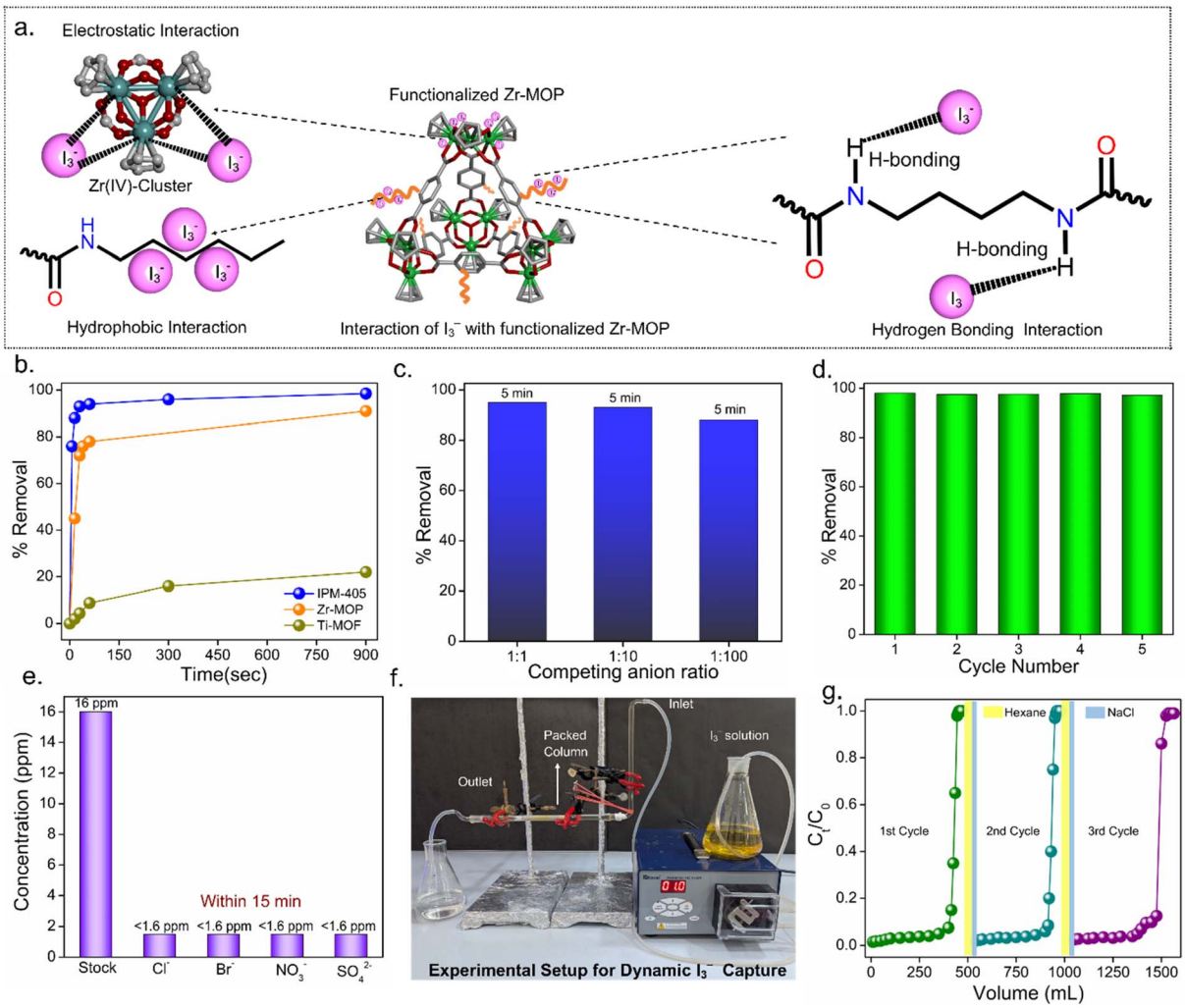

Fig. 3 (a) Interaction scheme of IPM-405 with I_3^- (b) I_3^- removal kinetics of IPM-405 along with Ti-MOF and Zr-MOP from water (for each case, 3 mg adsorbent in 3 ml of 100 ppm I_3^- solution was used). (c) Selective I_3^- removal study of IPM-405 in the presence of a large excess of counter anions (Cl^-, Br^-, NO_3^-, and SO_4^{2-}). (d) Regeneration ability of IPM-405 in the aqueous phase I_3^- removal study. (e) Ultra-trace selective I_3^- removal study of IPM-405. (f) Experimental setup for the dynamic flow through I_3^- removal study. (g) Aqueous phase I_3^- removal dynamic breakthrough profile of IPM-405.

important factor. Here, a multi-cycle triiodide removal study was performed on IPM-405, by regenerating the adsorbent with a solvent (see details in Section S6.6). It was found that the composite shows multiple operational cycles (Fig. 3d) without losing its performance, recognizing itself as a sustainable adsorbent for aqueous phase iodine removal. In actual cases, the concentration of iodine in wastewater remains below 10 ppm.[57] Therefore, the low/ultra-trace iodine (I_3^-) removal in the aqueous phase has been considered as an important remediation for iodine removal studies. However, it is challenging due to the lack of suitable iodine-selective functionality in the adsorbent. In the IPM-405 composite, the co-existence and synergistic action of all these functional and ionic moieties, and most importantly, their presence on the outer core of the porous host, make the composite highly recommended for the aqueous phase ultra-trace I_3^- removal study. The material was found to effectively remove >90% the ultra-trace I_3^- species from a mixed counter-anion polyiodide solution (16 ppm to <1.6 ppm) in just 15 min (Fig. 3e, S53 and 54) (see details in Section S6.5). Then, inspired by this highly selective, ultrafast, and ultra-trace iodine (I_3^-) removal ability of this composite, it was applied for dynamic column-based I_3^- separation from simulated wastewater under continuous flow-through conditions (Fig. 3g). The IPM-405 packed column efficiently removed iodine (I_3^-) under dynamic conditions (Fig. S55), maintaining effective removal over three consecutive cycles. IPM-405 established itself as a superior heterogeneous adsorbent platform for aqueous phase I_3^- removal even under dynamic flow-through conditions (Fig. 3f, see details in Section S6.7).

Iodine sorption mechanism study

The polyiodide sorption mechanism was studied, followed by a series of experiments implemented on I_3^-@IPM-405. The uniform distribution of iodine on the surface of the composite

after the aqueous phase iodine sequestration study was evidenced by FESEM-EDX and elemental mapping analysis (Fig. S56). The existence of I_3^- was also verified from the Raman spectra of I_3^-@IPM-405 (Fig. S63). To further support the presence of iodine, XPS analysis on the I_3^-@IPM-405 was performed. The XPS survey spectra also confirmed the presence of iodine in IPM-405 after the iodine sequestration study (Fig. S57). In the deconvoluted I 3d XPS spectra, two noticeable peaks were located at 618 eV & 630 eV, associated with the I 3d orbitals of tri-iodide species (Fig. S64). The absence of Cl^- in FESEM-EDX and in XPS analysis depicts ion exchange as one of the primary interaction mechanisms for tri-iodide (I_3^-) removal. In post-capture FT-IR analysis, the presence of all corresponding peaks indicates the retained framework integrity of the material after the iodine removal study (Fig. S58). The corresponding shift of the Zr–O band, secondary amide band, and alkyl C–H band was observed, which supports that these Zr-SBUs, secondary amide functionality, and hydrophobic long alkane chain moieties in the IPM-405 hybrid composite collectively interact with iodine (Fig. S59–S61).

Catalytic study

The presence of Lewis acidic center in the MOF creates a unique avenue in MOF-based heterogeneous catalysis.[64] In this context, the Zr(IV) cluster containing MOF reaffirmed its status as a well-known candidate in Lewis acid catalysis.[60,61] Alternatively, Zr(IV)-

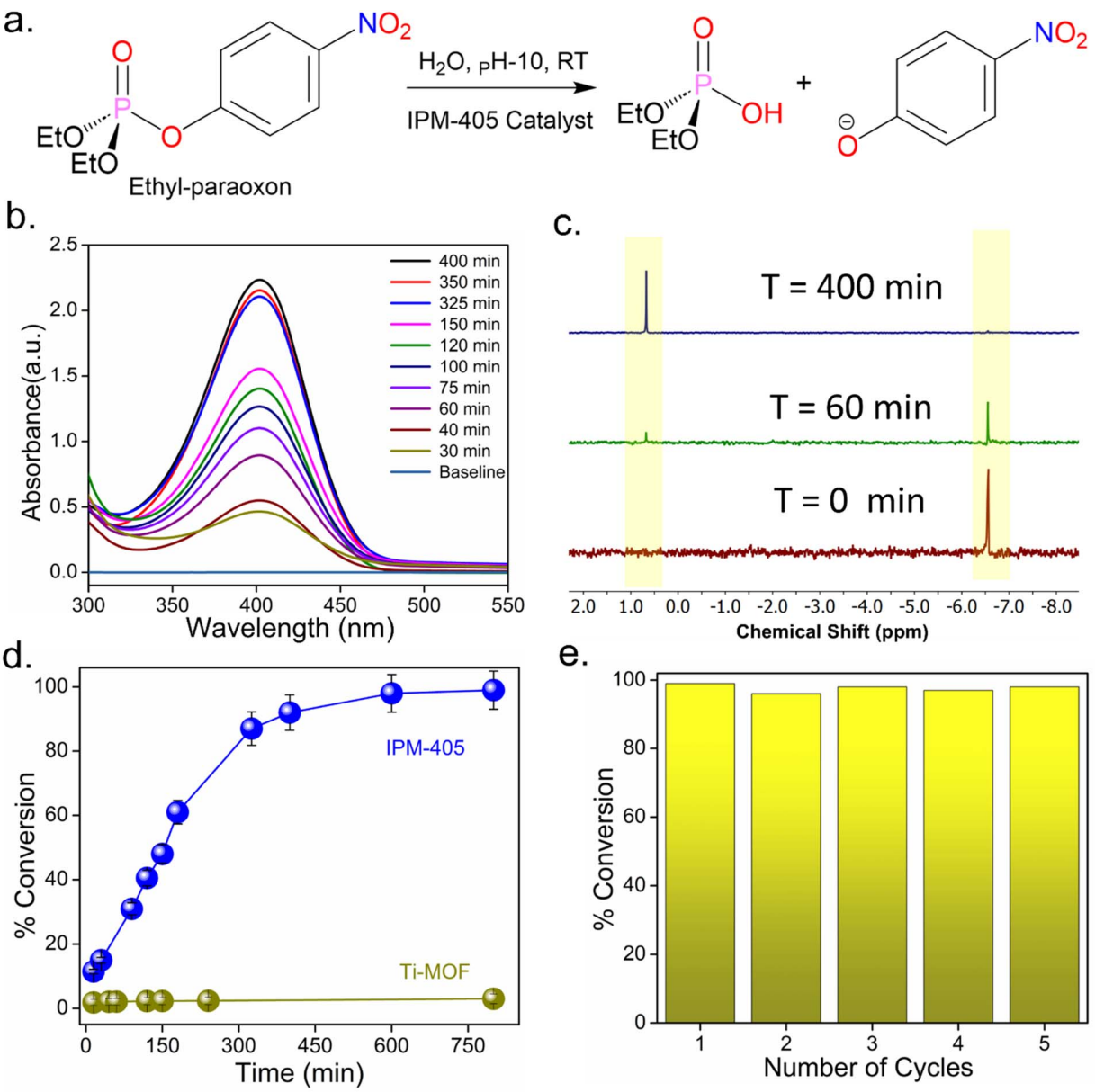

Fig. 4 (a) Hydrolysis reaction of ethyl-paraoxon at room temperature in the presence of the IPM-405 catalyst. (b) Time-dependent UV spectra and (c) ^{31}P-NMR spectra for the hydrolysis reaction of ethyl-paraoxon in the presence of IPM-405. (d) Degradation percentage of ethyl-paraoxon in the presence of IPM-405 and pristine Ti-MOF. (e) Multi-fold regeneration ability of IPM-405 for the hydrolysis reaction of ethyl-paraoxon.

based metal–organic polyhedra (MOPs), which also contain trinuclear Zr(IV) secondary building units, can serve as potential Lewis acid catalysts.[63] However, their solubility in organic solvents restricts their use as heterogeneous catalysts. Here, by the covalent grafting approach, the homogeneously distributed covalently anchored Zr(IV)-MOP surface of the composite stands as an effective solution to this problem. Here, through covalent grafting of the Zr-MOPs onto the outer surface of the Ti-MOF, the MOP molecules are immobilized, preventing them from dissolving in the organic solvent and enabling their use as a heterogeneous catalyst. To check this, as a proof of concept, we performed the Lewis acid-catalyzed phosphate-ester hydrolysis of ethyl-paraoxon (Fig. 4a). Ethyl paraoxon is classified as a highly toxic organophosphate pesticide due to the ease of transesterification of the P–O group of the nitrophenol under physiological conditions, posing a harmful risk to the human nervous system.[60–62] Here, the presence of Lewis acidic Zr(IV) center in the composite motivated us to perform the hydrolysis reaction of ethyl-paraoxon. As a result, it was observed that the IPM-405 composite was able to degrade ethyl paraoxon (95% degradation in 400 min) at room temperature (Fig. 4b–d) (see details in Section S7). On the flip side, the pristine Ti-MOF did not possess any Lewis acidic sites and therefore was found not to degrade ethyl paraoxon (Fig. 4d). The IPM-405 hybrid composite contains covalently grafted Zr-MOPs, which feature an intrinsic Lewis acidic Zr(IV)-oxo cluster. The presence of these effective Lewis acidic centers makes the composite a suitable catalyst for the ethyl paraoxon hydrolysis reaction. Thereafter, the recyclability study of IPM-405 for the paraoxon hydrolysis was performed (see details in Section S7). The composite was able to execute multi-fold operational cycles (Fig. 4e) for the Lewis acid-driven organophosphate hydrolysis reaction. While the pristine Zr-MOP functioned as a homogeneous catalyst for ethyl paraoxon degradation, the hybrid composite introduces a heterogeneous platform for this nerve agent hydrolysis reaction.

Conclusions

This work establishes a facile strategy for modulating the physicochemical properties of MOFs. On the other hand, in terms of MOPs, this synthetic approach offers a potential platform to expand the application of MOPs by minimizing their common drawbacks (aggregation-induced active site blockage and leaching issue in organic solvent) *via* the fabrication of a covalently grafted MOP-based porous hybrid composite. By covalent anchoring of these MOPs on the MOF outer surface, the activity of the MOPs is maximized while eliminating the leaching issue. The IPM-405 composite established itself as a crystalline functional ionic-porous hybrid adsorbent for ultrafast, ultra-trace, and selective removal of polyiodide species from the aqueous phase, which is important from the point of view of radioiodine sequestration from water. Also, the covalent grafting strategy depicts a fascinating route to introduce MOP-based heterogeneous catalysis as exemplified by Lewis-acid mediated phosphate-ester hydrolysis of toxic nerve agents. We believe that our synthetic strategy may be further adapted for other MOFs and MOPs to harness their full intrinsic potential.

Author contributions

D. G. and S. F. designed the project. D. G. synthesized and characterised the materials. D. G., K. B., A. R., and D. M. performed and analysed the capture study and catalytic study. D. G. and S. F. wrote the manuscript. All the authors reviewed the manuscript. S. K. G. supervised the project.

Conflicts of interest

There are no conflicts to declare.

Data availability

All data used for this study are available in the paper and supplementary information files (SI). Supplementary information is available. See DOI: **https://doi.org/10.1039/d5sc06370a**.

Acknowledgements

D. G., K. B. and A. R. acknowledge UGC for research fellowships. D. M. acknowledges IISER Pune for research fellowships. S. F. acknowledges the DST-Inspire (India) for the research fellowship (DST/INSPIRE/03/2016/001694). We are grateful to the IISER Pune for its research facilities. S. K. G. acknowledges DST-SERB (Project No. CRG/2022/001090) for funding.

Notes and references

1 A. G. Slater and A. I. Cooper, *Science*, 2015, **348**, aaa8075.
2 R. Freund, S. Canossa, S. M. Cohen, W. Yan, H. Deng, V. Guillerm, M. Eddaoudi, D. G. Madden, D. Fairen-Jimenez, H. Lyu, L. K. Macreadie, Z. Ji, Y. Zhang, B. Wang, F. Haase, C. Wöll, O. Zaremba, J. Andreo, S. Wuttke and C. S. Diercks, *Angew. Chem., Int. Ed. Engl.*, 2021, **60**, 23946–23974.
3 *Metal-Organic Frameworks (MOFs) for Environmental Applications*, ed. S. K. Ghosh, Elsevier Science Publishing, Philadelphia, PA, 2019.
4 S. Fajal, S. Dutta and S. K. Ghosh, *Mater. Horiz.*, 2023, **10**, 4083–4138.
5 J. Liu, L. Chen, H. Cui, J. Zhang, L. Zhang and C.-Y. Su, *Chem. Soc. Rev.*, 2014, **43**, 6011–6061.
6 (*a*) Y. Song, J. Phipps, C. Zhu and S. Ma, *Angew. Chem., Int. Ed. Engl.*, 2023, **62**, e202216724; (*b*) M. Dittmar, *Energy*, 2012, **37**, 35–40.
7 S. Rojas and P. Horcajada, *Chem. Rev.*, 2020, **120**, 8378–8415.
8 A. Bavykina, N. Kolobov, I. S. Khan, J. A. Bau, A. Ramirez and J. Gascon, *Chem. Rev.*, 2020, **120**, 8468–8535.
9 W. Mandal, S. Fajal, A. V. Desai and S. K. Ghosh, *Coord. Chem. Rev.*, 2025, **524**, 216326.
10 A. J. Gosselin, C. A. Rowland and E. D. Bloch, *Chem. Rev.*, 2020, **120**, 8987–9014.

11 J. Liu, Z. Wang, P. Cheng, M. J. Zaworotko, Y. Chen and Z. Zhang, *Nat. Rev. Chem.*, 2022, **6**, 339–356.
12 E. Sánchez-González, M. Y. Tsang, J. Troyano, G. A. Craig and S. Furukawa, *Chem. Soc. Rev.*, 2022, **51**, 4876–4889.
13 J. Albalad, L. Hernández-López, A. Carné-Sánchez and D. Maspoch, *Chem. Commun.*, 2022, **58**, 2443–2454.
14 A. Khobotov-Bakishev, L. Hernández-López, C. von Baeckmann, J. Albalad, A. Carné-Sánchez and D. Maspoch, *Adv. Sci.*, 2022, **9**, e2104753.
15 E. G. Percástegui, *Chem. Commun.*, 2022, **58**, 5055–5071.
16 C. T. McTernan, J. A. Davies and J. R. Nitschke, *Chem. Rev.*, 2022, **122**, 10393–10437.
17 S. Mollick, S. Fajal, S. Mukherjee and S. K. Ghosh, *Chem. Asian J.*, 2019, **14**, 3096–3108.
18 B. Lee, I.-H. Park and J. Park, *ACS Mater. Lett.*, 2022, **4**, 2388–2393.
19 B. Lee, B. Go, B. Jung and J. Park, *Small*, 2024, **20**, e2308393.
20 E.-S. M. El-Sayed, Y. D. Yuan, D. Zhao and D. Yuan, *Acc. Chem. Res.*, 2022, **55**, 1546–1560.
21 Z. Yang, S. B. Peh, S. Xi, Y. Lu, Q. Liu and D. Zhao, *Angew. Chem., Int. Ed. Engl.*, 2025, **64**, e202418098.
22 X. Feng, X. Wang, H. Yan, H. Liu, X. Liu, J. Guan, Y. Lu, W. Fan, Q. Yue and D. Sun, *Angew. Chem., Int. Ed. Engl.*, 2024, **63**, e202407240.
23 W. Fan, S. B. Peh, Z. Zhang, H. Yuan, Z. Yang, Y. Wang, K. Chai, D. Sun and D. Zhao, *Angew. Chem., Int. Ed. Engl.*, 2021, **60**, 17338–17343.
24 J. Liu, R. Zhang, X. Xie, J. Wang, F. Jin, Z. Wang, T. Wang, P. Cheng, J. Lu and Z. Zhang, *Angew. Chem., Int. Ed. Engl.*, 2025, **64**, e202414211.
25 C. R. Kim, T. Uemura and S. Kitagawa, *Chem. Soc. Rev.*, 2016, **45**, 3828–3845.
26 Q.-L. Zhu and Q. Xu, *Chem. Soc. Rev.*, 2014, **43**, 5468–5512.
27 G. Distefano, H. Suzuki, M. Tsujimoto, S. Isoda, S. Bracco, A. Comotti, P. Sozzani, T. Uemura and S. Kitagawa, *Nat. Chem.*, 2013, **5**, 335–341.
28 T. Kitao, Y. Zhang, S. Kitagawa, B. Wang and T. Uemura, *Chem. Soc. Rev.*, 2017, **46**, 3108–3133.
29 M. Kalaj, K. C. Bentz, S. Ayala Jr, J. M. Palomba, K. S. Barcus, Y. Katayama and S. M. Cohen, *Chem. Rev.*, 2020, **120**, 8267–8302.
30 V. J. Pastore and T. R. Cook, *Chem. Mater.*, 2020, **32**, 3680–3700.
31 Y. Li, M. Karimi, Y.-N. Gong, N. Dai, V. Safarifard and H.-L. Jiang, *Matter*, 2021, **4**, 2230–2265.
32 X. Qiu, W. Zhong, C. Bai and Y. Li, *J. Am. Chem. Soc.*, 2016, **138**, 1138–1141.
33 S. Fajal, W. Mandal, S. Mollick, Y. D. More, A. Torris, S. Saurabh, M. M. Shirolkar and S. K. Ghosh, *Angew. Chem., Int. Ed. Engl.*, 2022, **61**, e202203385.
34 W. Mandal, S. Fajal, D. Majumder, A. Sengupta, S. Let, R. R. Urkude, M. M. Shirolkar, A. Torris and S. K. Ghosh, *Chem. Sci.*, 2024, **15**, 18463–18475.
35 S. Fajal, W. Mandal, A. Torris, D. Majumder, S. Let, A. Sen, F. Kanheerampockil, M. M. Shirolkar and S. K. Ghosh, *Nat. Commun.*, 2024, **15**, 1278.
36 D. Majumder, S. Fajal, M. M. Shirolkar, A. Torris, Y. Banyla, K. Biswas, S. Rasaily and S. K. Ghosh, *Angew. Chem., Int. Ed. Engl.*, 2025, **64**, e202419830.
37 S. Mollick, S. Fajal, S. Saurabh, D. Mahato and S. K. Ghosh, *ACS Cent. Sci.*, 2020, **6**, 1534–1541.
38 Y. Liang, X. Yang, X. Wang, Z.-J. Guan, H. Xing and Y. Fang, *Nat. Commun.*, 2023, **14**, 5223.
39 Y. Liang, G. Xie, K.-K. Liu, M. Jin, Y. Chen, X. Yang, Z.-J. Guan, H. Xing and Y. Fang, *Angew. Chem., Int. Ed. Engl.*, 2025, **64**, e202416884.
40 H. Jiang, D. Alezi and M. Eddaoudi, *Nat. Rev. Mater.*, 2021, **6**, 466–487.
41 H. Furukawa, K. E. Cordova, M. O'Keeffe and O. M. Yaghi, *Science*, 2013, **341**, 1230444.
42 B. Li, H.-M. Wen, Y. Cui, W. Zhou, G. Qian and B. Chen, *Adv. Mater.*, 2016, **28**, 8819–8860.
43 G. Liu, Y. Di Yuan, J. Wang, Y. Cheng, S. B. Peh, Y. Wang, Y. Qian, J. Dong, D. Yuan and D. Zhao, *J. Am. Chem. Soc.*, 2018, **140**, 6231–6234.
44 F. Vermoortele, M. Maes, P. Z. Moghadam, M. J. Lennox, F. Ragon, M. Boulhout, S. Biswas, K. G. M. Laurier, I. Beurroies, R. Denoyel, M. Roeffaers, N. Stock, T. Düren, C. Serre and D. E. De Vos, *J. Am. Chem. Soc.*, 2011, **133**, 18526–18529.
45 Y. Gu, Y.-N. Wu, L. Li, W. Chen, F. Li and S. Kitagawa, *Angew. Chem.*, 2017, **129**, 15864–15868.
46 M. A. Nasalevich, R. Becker, E. V. Ramos-Fernandez, S. Castellanos, S. L. Veber, M. V. Fedin, F. Kapteijn, J. N. H. Reek, J. I. van der Vlugt and J. Gascon, *Energy Environ. Sci.*, 2015, **8**, 364–375.
47 Y. Han, W. Huang, M. He, B. An, Y. Chen, X. Han, L. An, M. Kippax-Jones, J. Li, Y. Yang, M. D. Frogley, C. Li, D. Crawshaw, P. Manuel, S. Rudić, Y. Cheng, I. Silverwood, L. L. Daemen, A. J. Ramirez-Cuesta, S. J. Day, S. P. Thompson, B. F. Spencer, M. Nikiel, D. Lee, M. Schröder and S. Yang, *Nat. Mater.*, 2024, **23**, 1531–1538.
48 D. Nam, J. Huh, J. Lee, J. H. Kwak, H. Y. Jeong, K. Choi and W. Choe, *Chem. Sci.*, 2017, **8**, 7765–7771.
49 R. C. Ewing and F. N. von Hippel, *Science*, 2009, **325**, 151–152.
50 T. C. T. Pham, S. Docao, I. C. Hwang, M. K. Song, D. Y. Choi, D. Moon, P. Oleynikov and K. B. Yoon, *Energy Environ. Sci.*, 2016, **9**, 1050–1062.
51 Z. Zhang, X. Dong, J. Yin, Z.-G. Li, X. Li, D. Zhang, T. Pan, Q. Lei, X. Liu, Y. Xie, F. Shui, J. Li, M. Yi, J. Yuan, Z. You, L. Zhang, J. Chang, H. Zhang, W. Li, Q. Fang, B. Li, X.-H. Bu and Y. Han, *J. Am. Chem. Soc.*, 2022, **144**, 6821–6829.
52 J. Wang, Z. Li, Y. Wang, C. Wei, K. Ai and L. Lu, *Mater. Horiz.*, 2019, **6**, 1517–1525.
53 X. Zhang, J. Maddock, T. M. Nenoff, M. A. Denecke, S. Yang and M. Schröder, *Chem. Soc. Rev.*, 2022, **51**, 3243–3262.
54 W. Xie, D. Cui, S.-R. Zhang, Y.-H. Xu and D.-L. Jiang, *Mater. Horiz.*, 2019, **6**, 1571–1595.
55 A. Sen, S. Sharma, S. Dutta, M. M. Shirolkar, G. K. Dam, S. Let and S. K. Ghosh, *ACS Appl. Mater. Interfaces*, 2021, **13**, 34188–34196.

56 W. Zhou, A. Li, M. Zhou, Y. Xu, Y. Zhang and Q. He, *Nat. Commun.*, 2023, **14**, 5388.
57 N. Arora, T. Debnath, M. C. Senarathna, R. M. Johnson, I. G. Roske, G. A. Cisneros and R. A. Smaldone, *Chem. Sci.*, 2024, **15**, 3571–3577.
58 L. Xie, Z. Zheng, Q. Lin, H. Zhou, X. Ji, J. L. Sessler and H. Wang, *Angew. Chem., Int. Ed. Engl.*, 2022, **61**, e202113724.
59 M. Zhang, J. Samanta, B. A. Atterberry, R. Staples, A. J. Rossini and C. Ke, *Angew. Chem., Int. Ed. Engl.*, 2022, **61**, e202214189.
60 Z. Cheng, K. M. Fahy, G. W. Peterson, K. O. Kirlikovali and O. K. Farha, *Adv. Mater.*, 2025, e2413848.
61 N. S. Bobbitt, M. L. Mendonca, A. J. Howarth, T. Islamoglu, J. T. Hupp, O. K. Farha and R. Q. Snurr, *Chem. Soc. Rev.*, 2017, **46**, 3357–3385.
62 M. J. Katz, J. E. Mondloch, R. K. Totten, J. K. Park, S. T. Nguyen, O. K. Farha and J. T. Hupp, *Angew. Chem., Int. Ed. Engl.*, 2014, **126**, 507–511.
63 K. Kiaei, K. Brunson, A. Gładysiak, K. Smith, K. Hunter, A. Thomas, D. Radke, T. Zuehlsdorff and K. C. Stylianou, *J. Mater. Chem. A*, 2023, **11**, 14265–14271.
64 Z. Hu and D. Zhao, *CrystEngComm*, 2017, **19**, 4066–4081.
65 Y. Kim, K. Jin, I.-H. Park, S. Lee, J. Park and J. Park, *Chem. Eng. J.*, 2024, **484**, 149321.